

Detection of diffuse γ -ray emission near the young massive cluster NGC 3603

Rui-zhi Yang¹ and Felix Aharonian^{1, 2}

¹ Max-Planck-Institut für Kernphysik, P.O. Box 103980, 69029 Heidelberg, Germany.

² Dublin Institute for Advanced Studies, 31 Fitzwilliam Place, Dublin 2, Ireland.

Received: / Accepted:

ABSTRACT

We report the Fermi Large Area Telescope's detection of extended γ -ray emission towards the direction of the young massive star cluster NGC 3603. The emission shows a hard spectrum with a photon index of 2.3 from 1 GeV to 250 GeV. The large size and high luminosity of this structure make it unlikely a pulsar wind nebular. On the other hand the spatial correlation with the ionised gas indicate a hadronic origin. The total cosmic ray (CR) protons energy are estimated to be of the order 10^{50} erg assuming the γ -rays are produced in the interaction of CRs with ambient gas. The environment and spectral features show significant similarity with the Cygnus cocoon. It reveals that the young star clusters may be a γ -ray source population and they can potentially accelerate a significant fraction of the Galactic cosmic rays.

1. Introduction

The current paradigm of cosmic rays (CRs) postulates that the acceleration sites of CRs are supernova remnant (SNRs). However, the recent measurements of ^{60}Fe abundance in CRs (Binns et al. 2016) indicate that a substantial fraction of CRs could be accelerated in young OB star clusters and related super bubbles. Furthermore, the measurements of the Galactic diffuse γ -ray emission shows that the CRs have a similar radial distribution as OB stars rather than SNRs (Acero et al. 2016; Yang et al. 2016). On the other hand, super bubbles do have sufficient kinetic energy, supplied by supernova explosions therein or collective stellar winds, to provide the flux of locally measured CRs (Parizot et al. 2004). Meanwhile, these objects should be visible in γ -rays due to the fresh accelerated CRs interacting with ambient gas. So far the only detection of such sources is Cygnus cocoon. One should note that Cygnus OB system is by far not the most powerful young star cluster in our Galaxy.

To search other analogues we have chosen NGC 3603, which is densest young star cluster in our Galaxy. NGC 3603 locates about 7 kpc away from the solar system and it is the Galactic clone of the core of 30 Doradus in Large Magellanic cloud. Also, it is one of the most massive H II regions in our Galaxy (Moffat et al. 1994). The age of NGC 3603 is about 2 Myr (Kudryavtseva et al. 2012). It contains more than 50 OB stars and Wolf-Rayet stars in a very compact region. These stellar winds from massive young stars provide sufficient kinetic energy to accelerated CRs. The weak non-thermal x-ray emission has been detected in this region as well (Moffat et al. 2002).

We have structured the paper as follows: in Section 2, we present the results of our analysis of the *Fermi*-LAT observations and discuss the observational uncertainties of the used procedure; In Section 3 we discuss the origin of the gamma-ray emission. We estimate the mass of gas in the based on the dust opacity maps, and derive the CR spectra and fluxes assuming that gamma-rays are produced in interactions of CR protons and nuclei with the ambient gas. In Section 4 we discussed other possible origin of the γ -ray emission; in Section 5 we present the main conclusion of this work.

2. Fermi LAT data analysis

2.1. Spatial analysis

We selected observations for which the *Fermi*-LAT detector was pointed towards NGC 3603 (MET 239557417 – MET 455067824), for a period of approximately 7 years. For this analysis, we have used the standard LAT analysis software package *v10r0p5*¹. Given the crowded nature of the region and to avoid systematic errors due to the poor angular resolution at low energies, as well as the domination of pulsar emission below several GeV in the Galactic plane, we selected only events with energies exceeding 10 GeV for the spatial analysis. The region-of-interest (ROI) was selected to be a $15^\circ \times 15^\circ$ square centred on the position of NGC 3603, i.e., $\text{ra}=168^\circ.848$, $\text{dec}=-61^\circ.251$. In order to reduce the effect of the Earth albedo background, we excluded from the analysis the time intervals when the Earth was in the field-of-view (specifically when the centre of the field-of-view was more than 52° from zenith), as well as the time intervals when parts of the ROI had been observed at zenith angles $> 100^\circ$. The spectral analysis was performed based on the P8_R2_v6 version of the post-launch instrument response functions (IRFs). Both the front and back converted photons were selected.

The γ -ray counts map above 10 GeV of the inner 5° is shown in the top left panel of figure.1. The identified Fermi LAT point sources listed in the 3rd Fermi source catalog (3FGL)(The Fermi-LAT Collaboration 2015) are also shown as red crosses. In this region pulsars dominate the point source population. There are also two unassociated Fermi point sources near NGC 3603, which are marked as green crosses in the figure. To derive the emission toward NGC 3603 we perform a likelihood analysis by using the tool *glike*. In the likelihood fitting we first include all the sources in the 3FGL catalog and the fermi diffuse background model *gll_iem_v06.fits* for the Galactic γ -ray emission, as well as the isotropic background model *iso_P8R2_SOURCE_V6_v06.txt*². The normalization and spectral index of the sources are left free in the analysis.

¹ <http://fermi.gsfc.nasa.gov/ssc>

² available at <http://fermi.gsfc.nasa.gov/ssc/data/access/lat/Back>

Table 1: Fitting results for different models

Model	-log(likelihood)	TS for the extended structure
diffuse model + 3FGL catalog	30637	
diffuse model + 3FGL catalog + Gaussian disk	30580	114
diffuse model + 3FGL catalog + five point sources	30613	

After the likelihood fitting we subtracted the best fit diffuse model and all the identified sources in the ROI, the resulted residual maps are shown in top right panel of figure. 1. We found strong residuals towards the direction of NGC 3603 (marked as purple diamond) and the unassociated Fermi source 3FGL 1111.9-6038. Slane et al. (2012) reveals that this source 3FGL 1111.9-6038 should be related to the supernova remnant MSH 11-62. The other unassociated Fermi source 3FGL 1112.0-6135, is not significant above 10 GeV and thus has little influence on the results. We then further subtracted the source 3FGL 1111.9-6038 and the residuals are shown in the bottom panel of Figure. 1. A diffuse emission peaks at the position of NGC 3603.

To study the morphology of the diffuse emission, we added a gaussian disk on top of the model used in the likelihood analysis. We then vary the position and size of the disk to find the best fit parameters. The best-fit result is a gaussian disk centered at (ra=167°.78, dec=-61°.28) with $\sigma = 1.1^\circ$, with a TS value of 114, corresponding to a significance of more than 10σ . We also test whether this extended emission is composed by several independent point sources. To do this we added 5 point source at the peaks in the residual maps. These point sources are not significant except for the one which coincide in position with NGC 3603. And the -log(likelihood) function value is larger than the gaussian disk case, even with more free parameters. Thus the point source scenario can be significantly excluded. We also note that the morphology of the residual reveal the hint for deviation from a simple gaussian disk, but the limited statistics prevent us to pursue this issue deeper. Thus in the following analysis we use the best-fit gaussian disk as the spatial template. We list the model and the -log(likelihood) value in Tab.1.

2.2. Spectral analysis

To obtain the spectral energy distribution (SED) of extended emission towards NGC 3603, we divided the energy range 1000 MeV–250 GeV into 8 logarithmically spaced bands and applied *glike* to each of these bands. The results of this analysis are shown in Figure 2. All data points have a test statistic (TS) values larger than 4, which corresponds to a significance of greater than 2σ . The spectral points can be well fitted with a power law with a photon index of 2.3. The power law spectrum extends to 250 GeV without any sign of cutoff. The total γ -ray luminosity above 1 GeV is 10^{36} erg given the distance of 7 kpc. In addition, we also plot the SED for the source 3FGL 1111.9-6038, which reveals a break above about 20 GeV.

3. CR accelerated in young star cluster

The young star cluster NGC 3603 contains more than 50 OB stars and Wolf-Rayet stars (Moffat et al. 1994), the collective wind or historical supernova explosion inside the cluster make it a potential accelerator of CRs (Parizot et al. 2004). The hard γ -ray emission has already been detected in the young star association Cygnus OB2 (Ackermann et al. 2011). NGC 3603 has more OB stars and a much denser star distribution compared to Cygnus OB2, which provide enough kinetic energy in the stellar

wind and make it a even more powerful acceleration site. Thus a natural explanation of the extended γ -rays are the fresh accelerated CRs illuminating the ambient gas.

The gas content can be investigated by various tracers. The traditional tracers of the hydrogen in the atomic and molecular forms are the 21 cm H I and 2.6 mm CO lines, respectively. In this paper we use the data from CO galactic survey of Dame et al. (2001) with the CfA 1.2m millimetre-wave Telescope, and the Leiden/Argentine/Bonn (LAB) Survey on H I gas. For the CO data, we use the standard assumption of a linear relationship between the velocity-integrated CO intensity, W_{CO} , and the column density of molecular hydrogen, $N(H_2)$. The conversion factor X_{CO} is chosen to be $2.0 \times 10^{20} \text{ cm}^{-2} (\text{K km s}^{-1})^{-1}$ as suggested by Dame et al. (2001); Bolatto et al. (2013). For the H I data we use the equation

$$N_{H I}(v, T_s) = -\log \left(1 - \frac{T_B}{T_s - T_{bg}} \right) T_s C_i \Delta v, \quad (1)$$

where $T_{bg} \approx 2.66$ K is the brightness temperature of the cosmic microwave background radiation at 21cm, and $C_i = 1.83 \times 10^{18} \text{ cm}^2$. In the case when $T_B > T_s - 5$ K, we truncate T_B to $T_s - 5$ K; T_s is chosen to be 150 K. The systematic uncertainties due to the different spin temperatures are discussed in Ackermann et al. (2012) and Acero et al. (2016) and the effect is quite small in most regions of the sky. Hummel et al. (2015) has revealed that for NGC 3603 most of the CO emission fall into the velocity of 0 – 20 km/s. We also use this range to integrate the line emission both of CO and 21 cm in this velocity range.

For different reasons, the neutral gas cannot be always traced by CO and H I observations (Grenier et al. 2005). In such cases (e.g. in optically thick clouds), the infrared emission from cold interstellar dust provides an alternative and independent measurements of the gas column density. To find it, we need a relation between the dust opacity and the column density. According to Eq. (4) of Planck Collaboration et al. (2011),

$$\tau_M(\lambda) = \left(\frac{\tau_D(\lambda)}{N_H} \right)^{dust} [N_{HI} + 2X_{CO}W_{CO}], \quad (2)$$

where τ_M is the dust opacity as a function of the wavelength λ , $(\tau_D/N_H)^{dust}$ is the reference dust emissivity measured in low- N_H regions, W_{CO} is the integrated brightness temperature of the CO emission, and $X_{CO} = N_{H_2}/W_{CO}$ is the H_2/CO conversion factor. The substitution of the latter into Eq. (2) gives

$$N_H = N_{HI} + 2N_{H_2} = \tau_m(\lambda) \left[\left(\frac{\tau_D(\lambda)}{N_H} \right)^{dust} \right]^{-1}. \quad (3)$$

Here for the dust emissivity at 353 GHz, we use $(\tau_D/N_H)_{353 \text{ GHz}}^{dust} = 1.18 \pm 0.17 \times 10^{-26} \text{ cm}^2$ taken from Table 3 of Planck Collaboration et al. (2011). Generally, the dust opacity is considered as a robust and reliable estimate of the gas column density. On the other hand, the dust opacity maps do not contain any information on the distance. Thus the column derived from dust opacity is the integration over the whole line of sight and should be regarded as an upper limit.

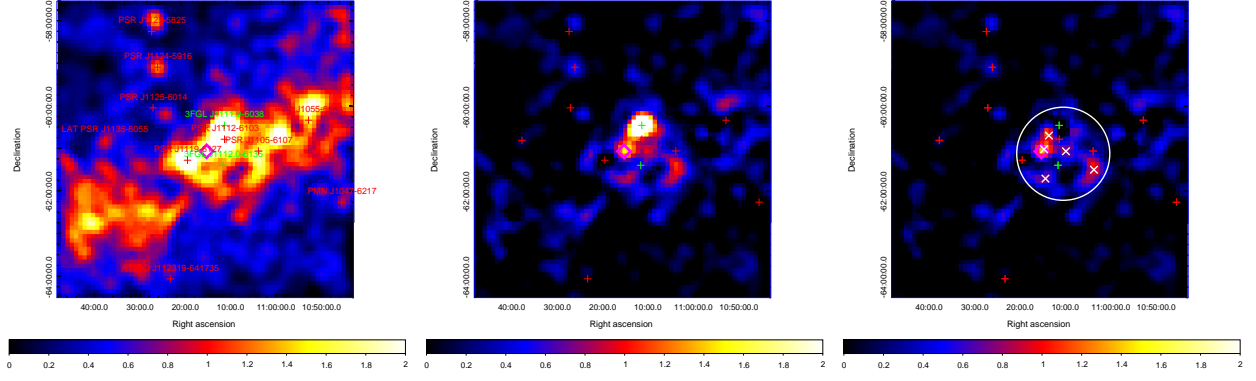


Fig. 1: *left* γ -rays counts map above 10 GeV in the inner 5° around NGC 3603. The identified 3FGL catalog sources are labeled as red crosses. The two unassociated catalog sources are labeled as green cross. The position of NGC 3603 is marked as a magenta diamond. *middle* : The residual map after subtracting all the identified catalog source and the diffuse background. *right* : The residual map after subtracting all the identified catalog source and the diffuse background, as well as the unassociated catalog source 3FGL 1111.9-6038. Also shown is the best fit gaussian disk (white circle, the radius is corresponding to the 1σ of the Gaussian) and the position of the five point sources (white "x") used to test the hypothesis that the extended emission comes from several independent point sources.

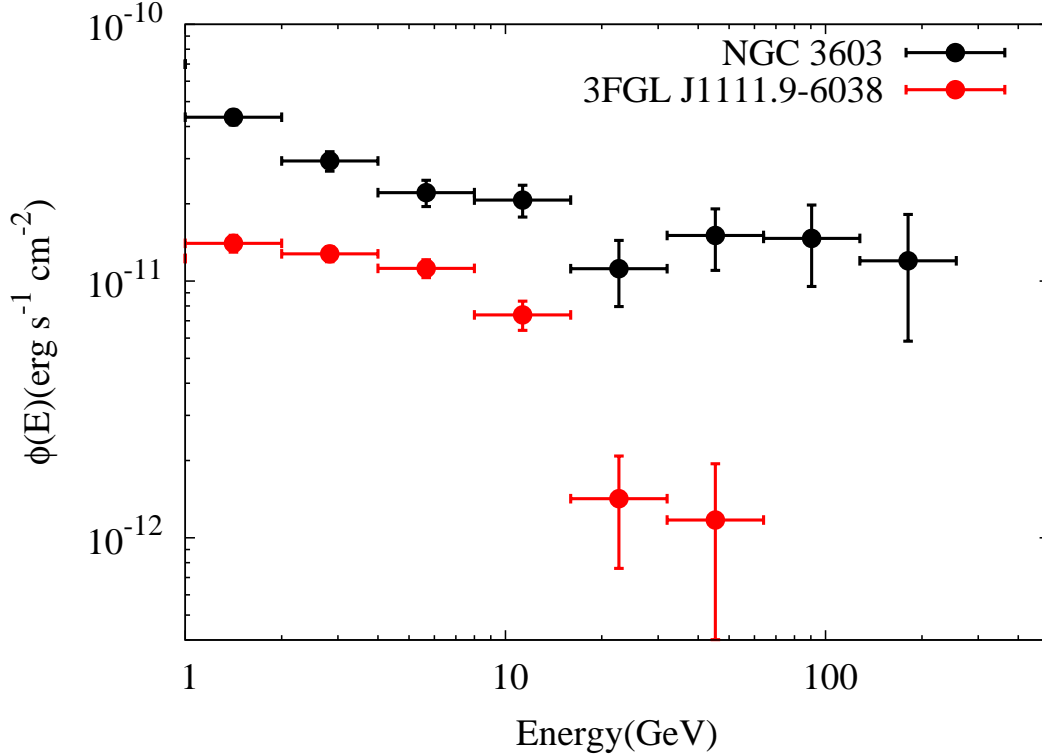


Fig. 2: The SEDs of the extended emission towards NGC 3603 and 3FGL 1111.9-6038.

NGC 3603 is the most massive H II region in the Galaxy. To determine the H II column we used the planck free-free map (Planck Collaboration et al. 2016). We first converted the emission measure (EM) in the planck map into free-free intensity by using the conversion factor in Table 1 of Finkbeiner (2003). Then we used Eq.(5) of Sodroski et al. (1997) to calculate the H II column from free-free intensity. We noted that the derived H II column is inverse proportional to electron density n_e , which are chosen to be 2 cm^{-3} and 10 cm^{-3} as an upper and lower limit here.

The derived gas column of all three phases are shown in Fig.3. We noted that the γ -ray emission shows good spatial correlation with the H II map, which support the hypothesis that the emission comes from the interaction of the fresh accelerated CRs with the ambient gas in the super bubble. The mass of gas corresponding to the diffuse emission can be determined from the gas column by assuming a distance of 7 kpc. The derived mass for different traces are listed in Table.2. As mentioned above, the mass derived from dust opacity can be regarded as an upper limit. The lower limit of the mass can be estimated as the

summation of the H I and H₂ mass, as well as the H I assuming $n_e = 10 \text{ cm}^{-3}$. Thus the total mass can be estimated in the range $2.2 \times 10^6 M_\odot < M < 12.0 \times 10^6 M_\odot$. If we assume the γ -ray emission region is spherical in geometry and the radius can be estimated as $r = D \theta \sim 7.0 \text{ kpc} \times (1.1/57.29) \text{ rad} \sim 130 \text{ pc}$. Thus the average volume gas density is $10 \text{ cm}^{-3} < n_{\text{gas}} < 60 \text{ cm}^{-3}$. Taken into account the total γ -ray luminosity of 10^{36} erg/s , one derive the total CR content in this area of $2 - 10 \times 10^{49} \text{ erg}$ assuming all γ -rays have a hadronic origin. This value is comparable to the total CR content in the Cygnus cocoon estimated as $1.3 \times 10^{49} \text{ erg}$ (Ackermann et al. 2011).

4. Other possible origins of the extended γ -ray emission

The regions near NGC 3603 is very crowded with several pulsars and supernova remnants. The γ -ray emission from pulsars typically has a cutoff at several GeV thus hardly can contribute to the hard γ -rays detected in the extended structures. However, the pulsar wind nebulae (PWN) and supernova remnant (SNR) can be natural contributors to hard γ -rays. We might expect some contribution also from the enhanced diffuse emission of this region. Furthermore, due to the crowded nature and the limited understanding of the interstellar medium in this region also introduce large uncertainty of the modeling of the Galactic diffuse γ -ray background. In this case the residuals may be due to the imperfect modeling of the diffuse background. Below we investigated the three possibilities in detail.

4.1. SNRs

There are three SNRs located inside the γ -ray emission region, SNR G290.1-0.8 (MSH 11-61A) (Slane et al. 2002), G291.0-0.1 (MSH 11-62) (Slane et al. 2012) and G292.2-0.5 (Ng et al. 2012). All three SNRs has a much smaller radio size compared to the size of the detected extended γ -ray emission. Furthermore, the age of SNR G290.1-0.8 and SNR G291.0-0.1 are 6000 and 1900 years, respectively. In such a short time scale the CRs cannot propagate more than 100 pc even if we assume a diffusion coefficient of $10^{29} \text{ cm}^2/\text{s}$, which is the typical value in the Galactic plane, near the SNRs. Indeed, due to the more turbulent environment near SNRs a much slower diffusion is predicted. G292.2-0.5, with a age of more than 2×10^4 years, is old enough for the accelerated CRs to occupy the γ -ray emission region.

4.2. PWNs

There are in total 8 pulsars which coincide with the γ -ray emission region. 5 of them are old with a rather low spin down luminosity ($< 10^{34} \text{ erg}$). The remaining three are PSR J1105-6107, J1112-6103 and J1119-6127. Neither of them can produce the extended γ -ray emission in their wind nebulae. First of all, the size of the structure, which is more than 100 pc, can hardly be produced by young pulsars. Thus PSR J1119-6127 with a age of only 1600 years (Camilo et al. 2000) can be excluded. The PWN of PSR J1105-6107 has been detected in x-ray (Gothelf & Kaspi 1998) and radio (Stappers et al. 1999), but with an angular size which is order of magnitude smaller. Prinz & Becker (2015) have performed a x-ray search for all the pulsars and found no evidence towards the direction of PSR J1112-6103. We cannot formally rule out a PWN from a yet undiscovered pulsar, in particular in these crowded region, but the correlation between the

γ -ray emission and the H II structure in NGC 3603 favours a CR origin.

4.3. imperfect modeling of diffuse background

The Galactic diffuse γ -ray background of Fermi LAT is produced by using GALPROP code (Vladimirov et al. 2011). In the previous analysis various point sources concentrated in the galactic plane has been founded and regarded to be related with the imperfect modelling of the galactic diffuse background, which as labeled as "c" in the Fermi catalog (The Fermi-LAT Collaboration 2015). Near NGC 3603 there are no such sources. On the other hand, in the Fermi Galactic diffuse background models, the γ -rays associated with ionised gas are not included (Acero et al. 2016). As mentioned in last section, NGC 3603 is the most massive H II region in the Galaxy. Thus the ignorance of H II gas may underestimate the γ -ray flux towards this direction significantly. However, the hard spectrum with an index of 2.3 is not compatible with the Galactic diffuse γ -ray background which has an index of 2.7, which is mainly contributed by the CR interaction with gas. We plot in Figure.4 the SED of NGC 3603 together with predicted γ -ray emission in the H II region assuming the CR density therein is identical to the density in the solar system measured by AMS-02 (Aguilar et al. 2015). The observed flux is twice higher than the predicted one at 1 GeV and nearly 2 orders of magnitude higher at 200 GeV. Thus the extended emissions are unlikely to related to the diffuse background components.

5. Reanalysis of PASS 8 data on Cygnus cocoon

Cygnus cocoon (Ackermann et al. 2011) is the first detected extended γ -ray emission near young star clusters. The γ -ray emission has a hard spectrum with a photon index of -2.1 up to 100 GeV and has a n angular extension of 2° . The hard spectrum of Cygnus cocoon reported by Ackermann et al. (2011) shows a similarity with NGC 3603. To take advantage of the accumulated exposure and developed understanding of instrument response, we reanalysis the region using 7 years PASS 8 Fermi LAT data (MET 239557417 – MET 455067824) with the latest LAT analysis software package *v10r0p5*. Cygnus cocoon is already included in the 3FGL template and we use the spatial templates therein. We divided the energy range 1000 MeV–500 GeV into 9 logarithmically spaced bands and applied *gtlike* to each of these bands. The derived SED of Cygnus cocoon are shown in Fig.5. The spectrum above 1 GeV can be well fitted with a power law with a photon index of 2.3. The detected spectrum extends to 500 GeV, without a clear sign of cutoff. The corresponding CR energy is up to 10 TeV if the γ -rays are produced by CR interaction with gas.

6. Discussion and conclusion

Originally, Binns et al. (2005) and Rauch et al. (2009), based on the composition of CRs, proposed that Galactic CRs are produced in the supper bubbles close to OB associations/star-clusters. The recent observations of ^{60}Fe in CRs provide a new support of this hypothesis (Binns et al. 2016). Furthermore, the measurement of γ -ray emissivities reveal a similar radial distribution of CRs with OB stars (Acero et al. 2016; Yang et al. 2016). If CRs are accelerated in such environment, high energy gamma-rays are expected from the interactions of the fresh accelerated CRs with the ambient gas. However up to now the only γ -ray detection towards these structures are Cygnus cocoon

Table 2: Gas mass derived from different tracers

Tracer	gas phase	mass ($10^6 M_\odot$)
Dust opacity	Total	12.0
21 cm + 2.6 mm line	H I + H ₂	1.7
free-free intensity ($n_e = 2 \text{ cm}^{-3}$)	H II	2.5
free-free intensity ($n_e = 10 \text{ cm}^{-3}$)	H II	0.5

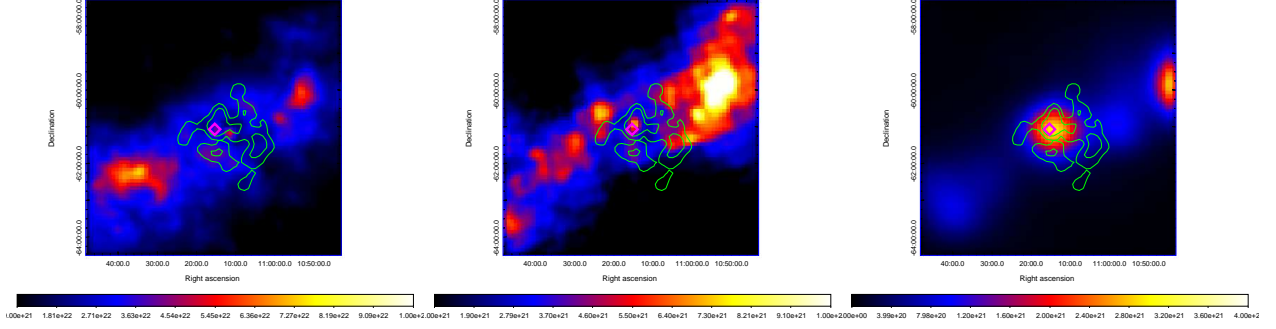


Fig. 3: *left*: Gas column derived from Planck dust opacity maps. *middle*: Gas column derived from 21cm and CO data, the velocity range of 0 – 20 km/s are chosen to integrate. *right*: The H II column derived from the Planck free-free maps.

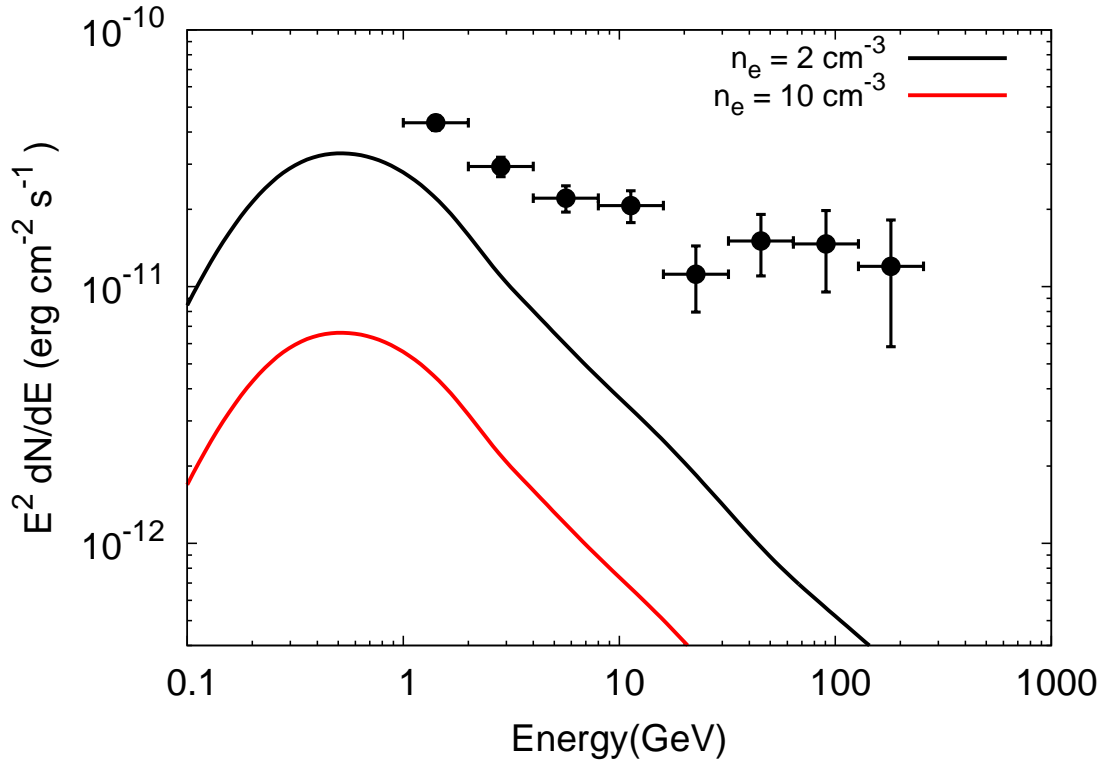


Fig. 4: The SEDs of the extended emission towards NGC 3603 together with the predicted γ -ray emission in the H II region assuming the CR density therein is identical to the density in the solar system measured by AMS-02 (Aguilar et al. 2015). The H II density are derived by using equation.5 of Sodroski et al. (1997) and free-free intensity from Planck Collaboration et al. (2016). The electron density n_e are chosen to be 2 cm^{-3} and 10 cm^{-3} , as shown in black and red curve, respectively.

(Ackermann et al. 2011). Here, we report a statistically significant detection of an extended gamma-ray signal from the direction of another star burst region, NGC 3603. Like the Cygnus cocoon, the spectrum of this source is hard, and extends up to 500 GeV. We argue that the most likely origin of the detected

emission is the interactions of CRs accelerated by stellar winds with the ambient gas. .

In addition to the Cygnus cocoon and NGC 3603, there are a few more similar objects like Westerlund 1, Westerlund 2, RSSG1, RSSG2, RSSG3 (for a review, see Portegies Zwart et al.

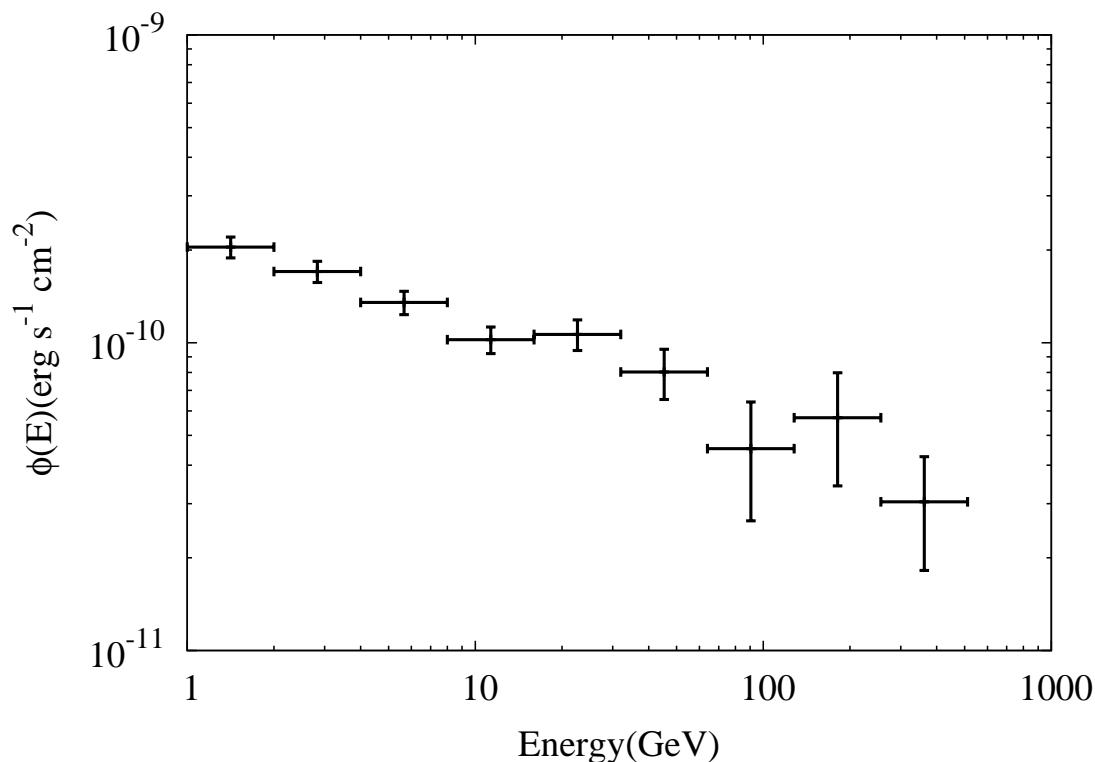


Fig. 5: The SEDs of cygnus cocoon.

2010), which can be considered as sites of CR accelerations and therefore as potential extended γ -ray sources. Interestingly, the first three of these objects have been reported as TeV gamma-ray emitters (Abramowski et al. 2012; H.E.S.S. Collaboration et al. 2011; Aharonian et al. 2006), thus it is likely that particles in these objects are accelerated to multi-TeV energies. In this regard a principal question is whether these objects can operate also as PeVatrons, i.e. whether they can provide the bulk of the locally observed CRs up to the so-called knee around 1 PeV.

The most straightforward and unambiguous answer to this question would be the detection of gamma-rays extending with a hard energy spectrum to energies well beyond 10 TeV. Apparently, because of the limited detection area, the Fermi LAT observations cannot offer such measurements. In this regard the Atmospheric Cherenkov Telescope Arrays with their huge detection areas and adequate angular and energy resolutions, are powerful tools for the search and study of cosmic PeVatrons. Remarkably, multi TeV-gamma-ray emission with a hard spectrum has been reported from Westerlund 1 by the HESS collaboration (Abramowski et al. 2012) which has been interpreted by Bykov (2014) as an indication of acceleration of protons in that object to PeV energies. However, this tentative result needs further confirmation.

The forthcoming Cherenkov Telescope Array (CTA), and to some extent also the water Cherenkov particle detectors like HAWK and LHAASO, are well designed for such studies.

References

Abramowski, A., Acero, F., Aharonian, F., et al. 2012, A&A, 537, A114
 Acero, F., Ackermann, M., Ajello, M., et al. 2016, ArXiv e-prints
 Ackermann, M., Ajello, M., Atwood, W. B., et al. 2012, ApJ, 750, 3
 Ackermann, M. et al. 2011, Science, 334, 1103

Aguilar, M., Aisa, D., Alpat, B., & et al. 2015, Physical Review Letters, 114, 171103
 Aharonian, F., Akhperjanian, A. G., Bazer-Bachi, A. R., et al. 2006, ApJ, 636, 777
 Binns, W. R., Israel, M. H., Christian, E. R., et al. 2016, Science, 352, 677
 Binns, W. R., Wiedenbeck, M. E., Arnould, M., et al. 2005, ApJ, 634, 351
 Bolatto, A. D., Wolfire, M., & Leroy, A. K. 2013, ARA&A, 51, 207
 Bykov, A. M. 2014, A&A Rev., 22, 77
 Camilo, F., Kaspi, V. M., Lyne, A. G., et al. 2000, The Astrophysical Journal, 541, 367
 Dame, T. M., Hartmann, D., & Thaddeus, P. 2001, ApJ, 547, 792
 Finkbeiner, D. P. 2003, ApJS, 146, 407
 Gotthelf, E. V. & Kaspi, V. M. 1998, ApJ, 497, L29
 Grenier, I. A., Casandjian, J.-M., & Terrier, R. 2005, Science, 307, 1292
 H.E.S.S. Collaboration, Abramowski, A., Acero, F., et al. 2011, A&A, 525, A46
 Hummel, C. A., Stanke, T., Galván-Madrid, R., & Koribalski, B. S. 2015, A&A, 582, A66
 Kudryavtseva, N., Brandner, W., Gennaro, M., et al. 2012, ApJ, 750, L44
 Moffat, A. F. J., Corcoran, M. F., Stevens, I. R., et al. 2002, ApJ, 573, 191
 Moffat, A. F. J., Drissen, L., & Shara, M. M. 1994, ApJ, 436, 183
 Ng, C.-Y., Kaspi, V. M., Ho, W. C. G., et al. 2012, ApJ, 761, 65
 Parizot, E., Marcowith, A., van der Swaluw, E., Bykov, A. M., & Tatischeff, V. 2004, A&A, 424, 747
 Planck Collaboration, Adam, R., Ade, P. A. R., et al. 2016, A&A, 594, A10
 Planck Collaboration, Ade, P. A. R., Aghanim, N., et al. 2011, A&A, 536, A19
 Portegies Zwart, S. F., McMillan, S. L. W., & Gieles, M. 2010, ARA&A, 48, 431
 Prinz, T. & Becker, W. 2015, ArXiv e-prints
 Rauch, B. F., Link, J. T., Lodders, K., et al. 2009, ApJ, 697, 2083
 Slane, P., Chen, Y., Lazendic, J. S., & Hughes, J. P. 2002, ApJ, 580, 904
 Slane, P., Hughes, J. P., Temim, T., et al. 2012, ApJ, 749, 131
 Sodroski, T. J., Odegard, N., Arendt, R. G., et al. 1997, ApJ, 480, 173
 Stappers, B. W., Gaensler, B. M., & Johnston, S. 1999, MNRAS, 308, 609
 The Fermi-LAT Collaboration. 2015, ArXiv e-prints
 Vladimirov, A. E., Digel, S. W., Jóhannesson, G., et al. 2011, Computer Physics Communications, 182, 1156
 Yang, R., Aharonian, F., & Evoli, C. 2016, Phys. Rev. D, 93, 123007